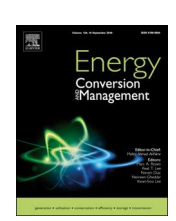
ELSEVIER

Contents lists available at ScienceDirect

# **Energy Conversion and Management**

journal homepage: www.elsevier.com/locate/enconman



# Bio-inspired bi-stable piezoelectric harvester for broadband vibration energy harvesting



Feng Qian<sup>a</sup>, Muhammad R. Hajj<sup>b</sup>, Lei Zuo<sup>a,\*</sup>

- <sup>a</sup> Department of Mechanical Engineering, Virginia Tech, Blacksburg, VA 24061, USA
- b Department of Civil, Environmental and Ocean Engineering, Stevens Institute of Technology, 1 Castle Point Terrace, Hoboken, NJ 07030, USA

#### ARTICLE INFO

#### Keywords: Vibration energy harvesting Bio-inspired design Piezoelectric Bi-stable Nonlinear dynamics

#### ABSTRACT

Inspired by the rapid shape transition of the Venus flytrap, a novel low-cost, bi-stable piezoelectric energy harvester is proposed, analyzed, and experimentally tested for the purpose of broadband energy harvesting. The harvester consists of a piezoelectric macro fiber composite (MFC) transducer, a tip mass, and two sub-beams with bending and twisting deformations created by pre-displacement constraints at the free ends using rigid tip-mass blocks. Different from bi-stable harvesters realized by nonlinear magnetic forces or residual stresses in laminate composites, the bio-inspired bi-stable piezoelectric energy harvester stores the potential energy induced by the mutual self-constraint of the sub-beams and harvests the large energy released during the rapid shape transition. Detailed design steps and principles are introduced and a prototype is fabricated to demonstrate and validate the concept. The experimentally measured nonlinear force-displacement curve of the harvester exhibits a discontinuous feature as the harvester jumps between the stable states. The dynamics of the proposed bio-inspired bi-stable piezoelectric energy harvester is investigated under sweeping frequency and harmonic excitations. The results show that the sub-beams of the harvester experience local vibrations including broadband high-frequency oscillations during the snap-through. The energy harvesting performance of the harvester is evaluated at different excitation levels over the frequency range of 9.0-14.0 Hz. Broadband energy harvesting is attained at relatively high excitation levels. An average power output of 0.193 mW for a load resistance of 8.2 k $\Omega$  is harvested at the excitation frequency of 10 Hz and amplitude of 4.0 g.

#### 1. Introduction

Energy harvesting from ambient environment has received increasing attention for the purpose of powering wireless sensors and low-power electronics. Because of its simplicity, the linear piezoelectric cantilever is the most widely studied energy transduction device for mechanical-to-electrical energy conversion [1]. However, linear piezoelectric energy harvesters are effective only over a very narrow frequency bandwidth, which leads to a significant efficiency reduction at frequencies slightly away from the resonant frequency [2,3]. Various approaches have been developed to broaden the operational frequency range of piezoelectric harvesters, such as frequency-up conversion [4], multiple resonator arrays [5], and exploitation of nonlinear responses [6]. Among the latter, nonlinear bi-stability has exhibited versatile features in harvesting energy from broadband vibrations due to the large power output associated with the global snap-through dynamics.

Bi-stable piezoelectric energy harvesters can be realized through different mechanisms, including mechanical preloading, magnetic

interaction, or residual thermal stress in laminate composite. Extensive reviews on bi-stable energy harvesting by exploiting different bi-stability mechanisms and transductions were published in [7,8]. Cottone et al. [9] used an axially loaded beam to form a buckled bi-stable piezoelectric vibration energy harvester that produced up to an order of magnitude more power than the unbuckled case. Ando et al. [10] and Qian et al. [11] exploited the bi-stable response of an axially pre-loaded clamped-clamped beam to the transverse excitations for piezoelectric energy harvesting over a wide frequency bandwidth. Harne et al. [12] developed a bi-stable energy harvesting device using an inertial mass connected to a translational slide bearing and a pre-compressed spring. The axial load leads to a negative stiffness that is sufficient to overcome the positive stiffness of the system and induces bifurcation via buckling. However, exerting a mechanical pre-load to a system usually involves additional constraints making the system clumsy. In comparison, magnetic interaction allows a more flexible design of bi-stable systems because of the contactless repulsive or attractive magnetic forces. The repulsive magnetic force between a fixed magnet and another one at the

E-mail address: leizuo@vt.edu (L. Zuo).

<sup>\*</sup> Corresponding author.

free end of a cantilever piezoelectric beam induces negative stiffness into the system and results in a bi-stable harvester [13,14]. Zhou et al. [15] used two tilted magnets and a cantilever beam with another tip magnet to build a bi-stable piezoelectric harvester. The inclination angle of the magnets was shown to play a vital role in broadening the operating bandwidth and enables rich nonlinear characteristics [16]. A magnetically coupled two-DOF bi-stable energy harvester consisting of two rotary piezoelectric cantilevers with tip magnets was investigated for energy harvesting from rotational motions of multiple frequency bands [17]. One disadvantage of magnet-based energy harvesters is that the magnetic field could interact with electronics and sensors to be powered. Bi-stability can also be realized by laminated composites where the residual thermal stress difference causes curvatures after the curing procedure from a high temperature to the room temperature due to the differing thermal expansion coefficients in different layers [18,19]. Syta et al. [20,21] investigated experimentally nonlinear dynamics of a bi-stable piezoelectric laminate plate and examined the modal response using Fourier spectrum based on the generated voltage time series. Firouzian-Nejad et al. [22,23] characterized the static snapthrough loads, out-of-plane displacement, curvature, and natural frequencies of bi-stable hybrid composite laminates by using experimental, analytical, and finite element methods. Pan et al. [24] investigated the influence of the layout of the hybrid symmetric laminates on the energy harvesting performance and the dynamics via finite element numerical analysis and experimental validation [25]. In addition to the complicated manufacturing process and high cost, laminate composites are sensitive to environmental moisture and temperature, resulting in changes in material properties especially for long-term services.

Bionic designs have been widely explored recently for the development of piezoelectric energy harvesting. By learning from the auditory hair bundle, a compliant bi-stable mechanism consisting of a fourbar linkage system was developed to enhance the performance of piezoelectric vibration energy harvesting [26]. Inspired by the structures of tree leaves, leaf-like piezoelectric harvesters composed of triangle polyvinylidene fluoride (PVDF) films and stiffeners mimicking bionic leaf veins were prototyped and tested for wind energy harvesting [27,28]. Enlightened by the parasitic relationship between a dodder and the host plant, a host-parasite piezoelectric energy harvester was proposed to achieve the bi-stability and frequency up-conversion for low-frequency, low-amplitude vibration energy harvesting [29]. A piezoelectric composite energy harvester was designed by imitating the unique microstructure of sea sponges, which has demonstrated remarkable improvements in vibration energy harvesting due to the welldistributed stress on the piezoelectric component [30]. This effort proposes a novel low-cost, magnet-free, bi-stable piezoelectric energy harvester inspired by the rapid shape transition of the Venus flytrap leaves. A cantilever beam is cut into two sub-beams, whose free ends are constrained by an in-plane pre-displacement to create the bending and twisting curves and to harvest the mechanical potential energy during the snap-through. The force-displacement relationship, nonlinear dynamics, and energy harvesting performance of the proposed bio-inspired bi-stable piezoelectric energy harvester are analyzed and experimentally investigated under different excitation frequencies and levels.

#### 2. Bio-inspired design

A good example of the bi-stable nonlinearity in nature is the Venus flytrap, which could trap agile insects by quickly closing its two curving leaves within a very short time (100 ms) [31]. The Venus flytrap leaves are bi-curved in two directions and have two layers of lopes with local tissues, porous structures, and fluid in between. The leaves will close when the inner layer contracts and outer layer stretches and will open in reverse, as shown in Fig. 1(a) and (b), respectively. The curved leaves are almost flat in the first stable (open) state and concave at the second

stable (close) state [32]. The plant achieves the open state by stretching its leaves back, during which the leaves store potential mechanical energy in the form of elastic energy. The stored energy will be released in the form of hydraulic movement in the porous structures when the leaves are triggered to snap shut. The rapid shape transition from the open state to the close state as the leaves sense external stimulus is referred to as the snap-through phenomenon. The sudden snap-through of a nonlinear bi-stable structure is usually associated with a large energy release, which results in large power output desired for vibration energy harvesting. If this snap-through mechanism could be used for energy harvesting, large power output can be achieved due to the concomitant higher energy release. In summary, the knowledge learned from the snap-through mechanism of the Venus flytrap includes: 1) the leaves are bi-curved in two directions, and 2) the leaves store potential mechanical energy.

Inspired by the rapid shape transition of the hyperbolic leaves of the Venus flytrap, a low-cost, magnet-free, bi-stable piezoelectric energy harvester is developed to harvest energy from broadband vibrations. The host structure of the proposed bio-inspired bi-stable piezoelectric energy harvester (BBPEH) is tailored from a cantilever beam, as illustrated in Fig. 2(a), by cutting off a strip in the middle of the beam along the length direction. The resultant structure has two sub-beams, as shown in Fig. 2(b), which are specifically inspired by the double-leaf structure of the Venus flytrap. The energy is harvested by bonding a piezoelectric transducer on the surface of one of the sub-beams near the clamped end, as displayed in Fig. 2(c). It is worth noting that more piezoelectric transducers could be attached to the other sub-beam or the opposite surface of the same sub-beam to improve the power output. To introduce the curvature in the length and width directions, an in-plane pre-displacement  $\Delta$  is applied oppositely to the two free ends of the sub-beams, which are then constrained by two rigid blocks, as depicted in Fig. 2(d). The in-plane pre-displacement is exerted along the width direction of the sub-beams towards to the cut-off middle strip as indicated by the two vectors in Fig. 2(d). It is worth mentioning that the pre-displacement should be less than the net distance between the two sub-beams to avert overlap.

These rigid blocks can also be used to tune the local resonant frequency of the nonlinear harvester. The in-plane pre-displacement constraint induces both bending and twisting deformations in the subbeams, therefore, curvatures in both the length and width directions. The deformed structure also stores the potential energy of bending and twisting deformations resulting from the applied pre-displacement constraint, which is analogous to the potential mechanical energy in the Venus flytrap. Since the bending and twisting deformations are achievable bi-directionally for the sub-beams, the structure has two stable states as illustrated in Fig. 2(e) and (f), respectively.

The proposed BBPEH satisfies the two conditions learned from the snap-through mechanism of the Venus flytrap. When the harvester is subjected to base excitations at the clamped end, it will vibrate either locally around one of the stable states (shown in Fig. 2(e) and (f)) or globally snap from one stable state to the other. The design takes full advantage of the mutual constraint and balance of the two sub-beam structures to achieve the self-twisting and pre-stress purpose. Compared with the bi-stable piezoelectric energy harvesters made of magnets [15,17] or composite laminates [20,21,25], the merits of the proposed BBPEH lie in its easy manufacturing, low-cost, and the elimination of the magnetic field, as usually used in previously proposed bi-stable energy harvesters. Since the proposed BBPEH does not need additional magnets and is simply made of metal sheet, the cost can be lower than the magnet- and composite laminate-based harvesters with the same piezoelectric MFC transducer. Additionally, the quickly snap-through motion between the two stable states can cause local high frequency vibrations of the sub-beams due to the sudden energy release. As such, even under a low-frequency excitation, the sub-beams can locally vibrate at very high frequencies because of the snap-through. This capability to convert low-frequency excitations to a high-frequency

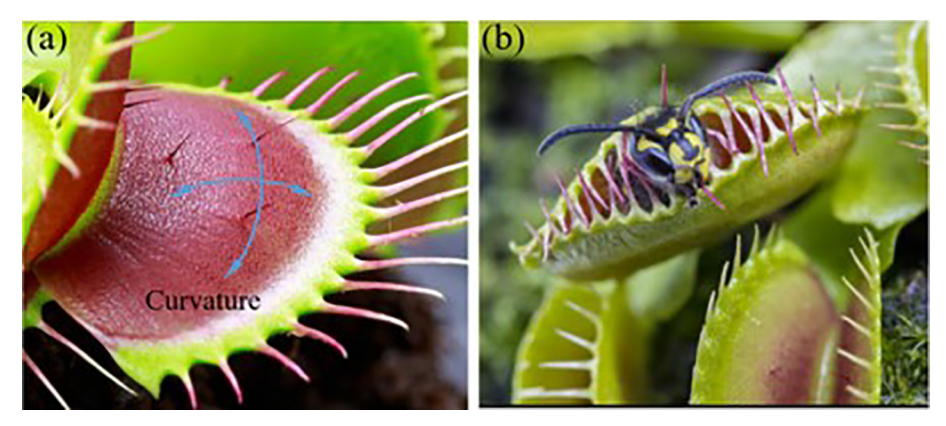
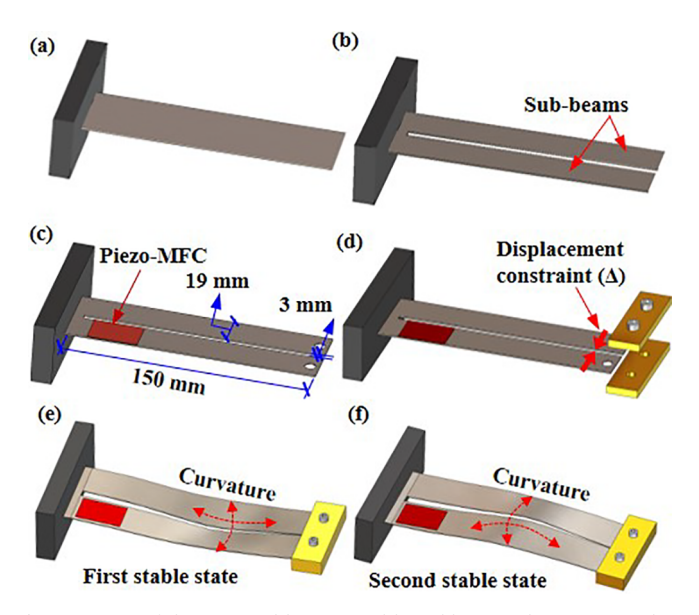


Fig. 1. Bistability of the Venus flytrap leaves which have bi-directional curves with stored mechanical potential energy: (a) first stable state when the two leaves open (b) second stable state when the two leaves close.



**Fig. 2.** Design of the proposed bio-inspired bi-stable piezoelectric energy harvester: (a) cantilever beam (b) tailored cantilever beam with two subbeams (c) the piezoelectric transducer was attached to one of the sub-beams to harvest vibration energy (d) applied in-plane displacement constraint (e) bi-curved subbeams under the applied constraint (first stable state) (f) second stable state.

vibrations has not been extensively explored but can be very effective to attain large power outputs especially when using piezoelectric transduction.

#### 3. Modeling and experimental tests

A prototype of the bi-stable piezoelectric harvester was built using a metal cantilever structure, piezoelectric macro fiber composite (MFC, M2814-P2, Smart Material Corp.), and two rigid copper blocks. Fig. 3(a) and (b) show the first and second stable states of the manufactured prototype of the BBPEH. The active length and width of the piezoelectric MFC are 28 mm and 14 mm, respectively. The thickness of the beam is 0.381 mm. The rest of the dimensions of the harvester are noted in Fig. 2(c).

## 3.1. Modeling

It is challenging to develop a rigorous analytical model to characterize the proposed BBPEH because of the irregular structure and complicated constraints. The dynamics of a bi-stable beam structure with the axial pre-stress can be described by a simplified lumped-mass

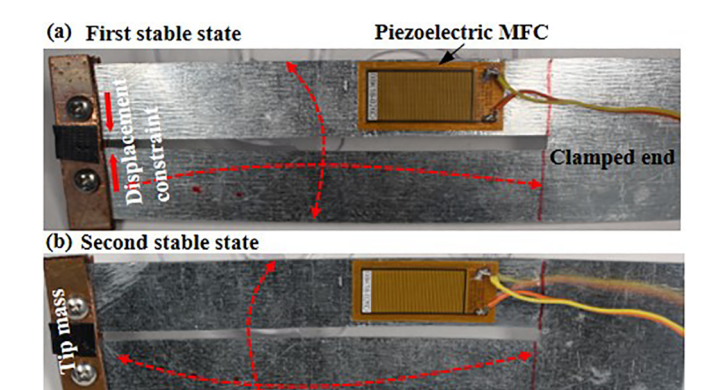


**Fig. 3.** The prototype of the proposed bio-inspired bi-stable piezoelectric energy harvester: (a) first stable state, (b) second stable state.

model with coupled higher-order terms induced by the axial motion [11,33]. The coupled governing mechanical and electrical equations are written as

$$\ddot{x} + 2\xi\omega_n\dot{x} + \beta(x\dot{x}^2 + x^2\ddot{x}) + f_{nl}(x) + \theta\nu + \bar{\theta}x^2\nu = -\mu\ddot{y}$$
 (1)

$$C_p \dot{v} + \frac{v}{R} - \theta \dot{x} - \alpha x^2 \dot{x} = 0$$
 (2)

where x and v are the tip displacement of the BBPEH and voltage output across the external resistive load R, the over dots indicate the derivatives with respect to time.  $\xi$  is the damping ratio,  $\beta$  and  $\alpha$  are the coefficient of the coupled higher order terms induced by the axial stresses,  $\theta$  and  $\bar{\theta}$  are the linear and nonlinear electromechanical coupling coefficients,  $\mu$  is the inertia force factor due to the distributed mass of the harvester,  $\ddot{y}$  is the base excitation acceleration,  $f_{nl}$  is the nonlinear restoring force, which contributes to the bi-stability due to the negative stiffness.  $C_p$  is the capacitance of the piezoelectric MFC, which is 48 nF as specified in the datasheet. It should be pointed out that the model considers the nonlinearity resulting from the pre-stress and the middle plane stretch of the beam but does not take the twisting motion into account. Below, using experimental results, it is shown that the system could be represented by this simplified single degree-of-freedom model with acceptable errors.

#### 3.2. Measurement of the force-displacement relationship

An experiment was carried out to derive the nonlinear restoring force curves describing the relation between the displacement and force. The experimental setup is shown in Fig. 4, in which a stander and a ball-screw mechanism were used to drive the force gauge (Mark-10 M2-2) forward and backward. The clamped end of the BBPEH was fixed

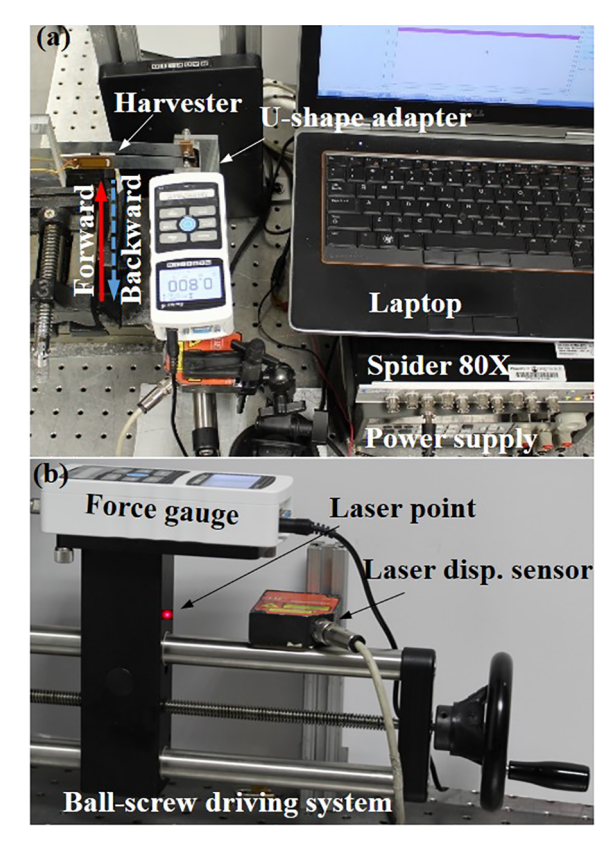


**Fig. 4.** Experimental setup of the force–displacement measurement: (a) overall experimental setup, (b) close-up view of the ball-screw driving system, laser displacement sensor, and force gauge.

to a support, and the free end was connected to the force gauge with a U-shape adapter and two pins. The two pins clip but do not hold tightly the free end of the harvester to allow the harvester to move freely in the axial direction as the free end is driven forward and backward by the force gauge. The laser displacement sensor (Micro Epsilon optoNCDT 1302) is used to measure the tip displacement of the harvester, which is the travel distance of the ball-screw. The Spider 80X (by Crystal Instruments Corp.) and laptop are used to collect the data from the displacement sensor. The force–displacement relationship was measured by driving the force gauge in both forward and backward directions, as indicated by the solid and dashed arrow lines in Fig. 4. When the force gauge moved forward the harvester snapped from the first stable state to the second one as shown in Fig. 3. By reversing the force direction, the harvester snapped from the second stable state back to the first one. The measured force was read directly from the force gauge.

The measured force–displacement variations are plotted in Fig. 5(a). The star and circle markers in the figure represent the measured data points as the force gauge moved forward and backward, respectively, while the curves are the fitted models with the sixth order polynomials.  $A_0$  and  $C_0$  mark the two equilibrium positions with the pentagrams corresponding to the two stable states, where the forces are zero. To measure the negative force (A-A<sub>0</sub>) in the experiment by driving the force gauge forward, the beam was pulled backward to a position in advance and was then gradually pushed forward by the force gauge. Similarly, to measure the positive force (C-C0) by driving the force gauge backward, the beam was firstly pushed to a position and was then slowly pulled backward. The force–displacement curves of the proposed BBPEH are quite different from that of a general bi-stable system, which usually characterized by one continuous force–displacement curve [34].

The nonlinear restoring force follows the  $A\text{-}A_0\text{-}B\text{-}B_0$  (C-C<sub>0</sub>-D-D<sub>0</sub>) branch as the force gauge moves forward (backward). The force firstly

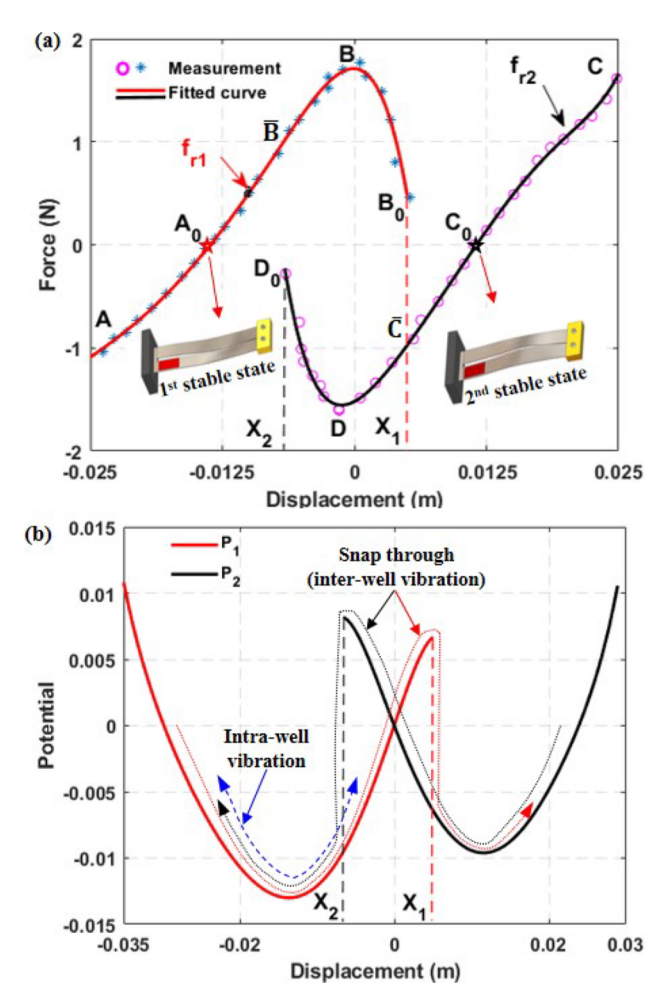


**Fig. 5.** Measurement of the nonlinear restoring force: (a) measured force-displacement curve, (b) the potential function of the BBPEH.

increases along with the displacement to a maximum value at B (D), after which it decreases due to the negative stiffness. The nonlinear restoring force causes the jump to the other branch at the point  $B_0$  ( $D_0$ ) if the displacement keeps on increasing and exceeds  $X_1$  ( $X_2$ ), which indicates that the harvester snapped from the first (second) stable state to the second (first) one. The harvester exhibits a softening stiffness from point  $A_0$  to A ( $C_0$  to C), hardening stiffness from point  $A_0$  to B ( $C_0$  to D), and negative stiffness from point B to  $C_0$  (D to  $C_0$ ).

The polynomial curve fittings of the nonlinear restoring forces are given by

$$\bar{f}_{nl}(x) = \begin{cases} f_{r1} = \sum_{i=0}^{6} k_{li} x^{i}, A - A_{0} - B - B_{0} \text{ branch} \\ f_{r2} = \sum_{i=0}^{6} k_{2i} x^{i}, C - C_{0} - D - D_{0} \text{ branch} \end{cases}$$
(3)

where the coefficients  $\{k_{1i},\ i=0,\ 1,\ 2,\ ...,6\}=[1.710,\ -6.016,\ -3.052\times 10^4,\ -2.816\times 10^6,\ -1.335\times 10^8,\ -3.363\times 10^9,\ -3.510\times 10^{10}],$  and  $\{k_{2i},\ i=0,\ 1,\ 2,\ ...,6\}=$  . It should be

[-1.520, 54.48, 1.798 × 
$$10^4$$
, 1.930 ×  $10^6$ , 1.296  
×  $10^8$ , -4.962 ×  $10^9$ , 7.605 ×  $10^{10}$ ]

noted that the measured or fitted restoring force  $\bar{f}_{nl}=mf_{nl}$ , where m is the effective mass of the harvester that can be identified from the local natural frequencies and the linear stiffness near the equilibrium positions. In the numerical integration, the nonlinear restoring force at each time step is determined from the displacement at the current time step and the restoring force at the previous one. For instance, if the displacement  $x(t_n)$  of the harvester at the current time step  $t_n$  is less than  $X_2$  the restoring force is  $f_{r1}$  along the branch A-A<sub>0</sub>-B-B<sub>0</sub>; while if the

**Table 1**Rule-base for the nonlinear restoring force *f*.

Displacement	$f_{\mathbf{r}}\left(x,t_{n-1}\right)$	$f_{\mathbf{r}}(x, t_n)$ and branch
$x(t_n) < X_2$	$f_{r1}$	$f_{r1}, A \to \bar{B} \text{ or } \bar{B} \to A$
$X_2 < x(t_n) < X_1$	$f_{r1}$	$f_{r1}, C \to \bar{B} \text{ or } \bar{B} \to C$
	$f_{r2}$	$f_{r2}$ , B $\rightarrow$ $\bar{C}$ or $\bar{C} \rightarrow B$
$x(t_n) > X_1$	$f_{r2}$	$f_{r2}$ , D $\rightarrow$ $\bar{C}$ or $\bar{C} \rightarrow D$

displacement is larger than  $X_1$ , the restoring force is  $f_{r2}$  along the branch C-C<sub>0</sub>-D-D<sub>0</sub>. It is more complicated when  $x(t_n)$  jumps between  $X_1$  and  $X_2$ , in which case the nonlinear restoring force depends on the force from the previous time step. If  $f_{nl}(x, t_{(n-1)}) = f_{r1}$ , which implies  $f_{nl}(x, t_{(n-1)})$  is on the branch A-A<sub>0</sub>-B-B<sub>0</sub>,  $f_{nl}(x, t_n) = f_{r1}$  at the current time step, otherwise,  $f_{nl}(x, t_n) = f_{r2}$ . Based on the analysis above, a rule-base for the nonlinear restoring force is established and used in the numerical integrations of Eqs. (1) and (2) as presented in Table 1.

This variation of the force-displacement curves is attributed to the boundary conditions, imperfect geometry properties, and asymmetrical stress distribution in the harvester. Similar force-displacement curves were also found in other bi-stable systems, such as the bi-stable composite structure [35] and shallow arch [36]. It was observed during the experiments that the large deformation firstly appeared close to the clamped end of the harvester and then gradually spread toward the free end as the forcing increased. The potential energy function of the BBPEH was obtained by integrating the fitted polynomials of the nonlinear restoring forces and plotted in Fig. 5(b), which suggests that the harvester has two asymmetric potential wells and independent barriers. The asymmetry in the potential wells results from the manufacturing error in the geometries of the two sub-beams and the effect of the piezoelectric MFC transducer. The trajectories of both the intra-well and inter-well motions of the BBPEH are illustrated in Fig. 5(b). An initial attempt has been given to build a FE model and simulate the bistable nonlinear behavior of the proposed BBPEH statically, which is desirable and valuable for the verification and parameter studies of the force-displacement curves. However, it's found that the pre-displacement constraint exerted by the rigid blocks at the free ends of the subbeams is very challenging to consider in the model. The rigid blocks not only purely apply the in-plane pre-displacement constraint, but also flatten out the twisted deformations at the free ends. As a result, all the degree-of-freedom at the free ends of the sub-beams have the same motion with the rigid tip mass. Another challenge is that the imperfect connection between the two rigid blocks and the free ends results in friction between the sub-beams and the blocks and consequently a big energy loss, which could be observed from the hysteretic behavior of the force-displacement curve. Nevertheless, numerically modeling the force-displacement relationship of the harvester by effectively taking these challenges into account will be the future research directions to fully understanding the nonlinear behaviors of the system.

The intra-well and inter-well dynamics of a bi-stable system primarily depend on the potential function apart from the external excitation. It is worth noting that the potential function, as well as the force-displacement curves of the proposed BBPEH, is set by the predisplacement  $\Delta$  once the geometric dimensions are given. Intuitively, exerting a larger pre-displacement  $\Delta$  to the free ends of the sub-beams needs more effort than applying a smaller one due to the larger restoring force. In principle, a larger  $\Delta$  injects more potential energy to the system in the form of larger stress and strain. This implies that the system created with a larger  $\Delta$  has deeper potential wells and higher barriers, and higher energy release accompanied by larger amplitude vibrations during the snapping through. However, bi-stable energy harvesting systems with deeper potential wells and higher barriers require larger external excitations to activate the desired snap-through dynamics when compared with the ones with lower potential wells. It has also been shown that the asymmetry in the two potential wells has a

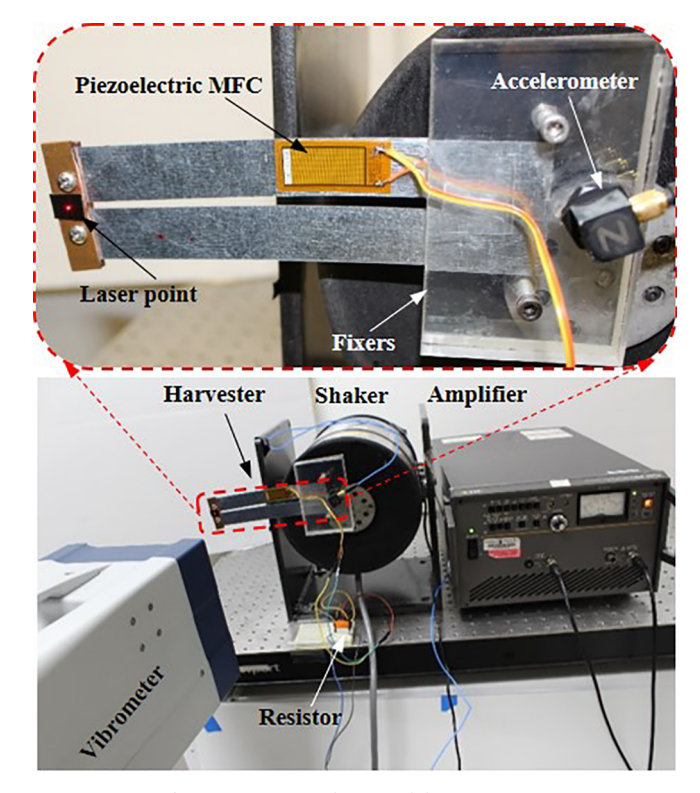


Fig. 6. Experimental setup of dynamics tests.

significant influence on the energy harvesting performance of bi-stable harvesters under random excitations [37]. The asymmetry in the potential wells degrades the mean power output for the random excitations of low to moderate noise intensities [38]. In the proposed BBPEH configuration, the asymmetry in the potential wells can be reduced or even eliminated by subtly tailoring the width of the sub-beams.

#### 3.3. Dynamics experimental setup

Experiments were conducted on the prototype to validate the design, identify the system parameters, and evaluate the energy harvesting performance of the proposed BBPEH. The experimental setup is shown in Fig. 6, where the harvester was fixed on a VT-600 shaker providing base excitations. A Polytech Laser Vibrometer (Model # PSV-500) was used to measure the tip velocity and to record the voltage output of the harvester. The input signal was generated from the laser vibrometer, amplified by an amplifier, and then fed to the shaker. The PCB accelerometer (PCB 356A17) was employed to measure the base excitation acceleration. Frequency sweep experiments were performed firstly with very low excitation levels (amplitudes) to identify the local resonant frequency  $\omega_n$  under the open circuit condition and the electromechanical coupling coefficient  $\theta$  of the harvester at the first stable state. The local vibration resonant frequency of the harvester was found to be  $\omega_n = 78.35$  rad/s. The remaining system parameters were identified from the frequency sweep experiment under a higher excitation given level and as follows:  $\xi = 5.6 \times 10^{-3}, \beta =$ 1.0,  $\theta = 2.821 \times 10^{-5}$ ,  $\bar{\theta} = 0.2$ ,  $\mu = 0.33$ , and  $\alpha = 6.08 \times 10^{-2}$ .

## 4. Results and discussion

#### 4.1. Frequency sweep excitations

The numerical integrations of the governing Eqs. (1) and (2) were performed using the input acceleration excitations measured from experiments. The nonlinear restoring force at each time step of the numerical integration was determined using the proposed rule-base in

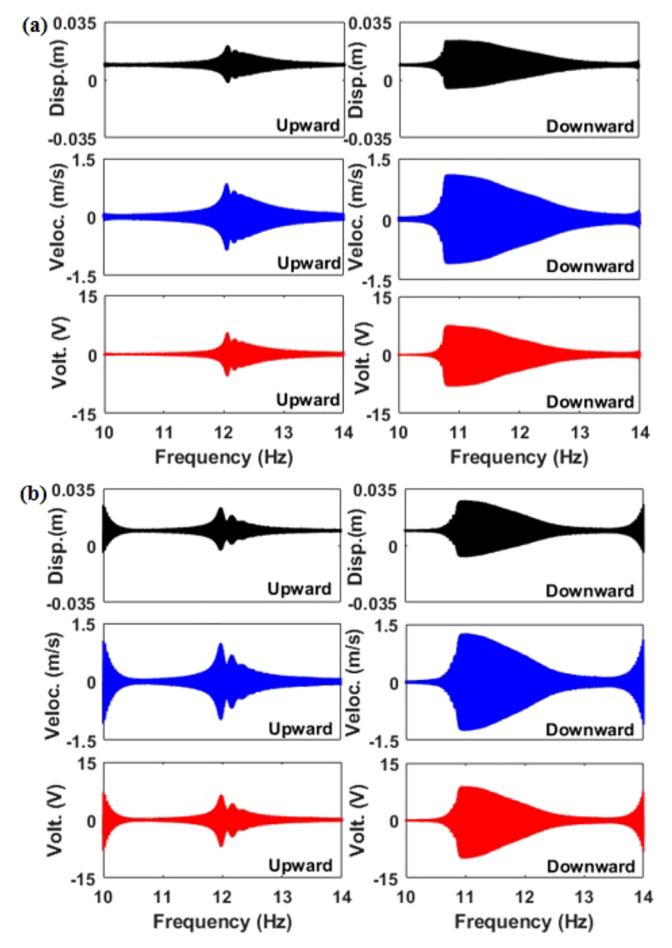


Fig. 7. Frequency sweep experiment results of intra-well vibrations: (a) experiment, (b) simulation.

Table 1. The excitation frequency linearly increases and decreases in the range of interest for the upward and downward frequency sweep experiments and numerical integrations. The measured excitation acceleration also linearly increases and decreases along with the upward and downward frequency sweeps. For the intra-well dynamics test, the excitation acceleration level is lower, between 0.35 g and 0.55 g, in comparison to 2.1 g to 4.1 g noted as the higher excitation level to activate the large amplitude inter-well vibrations. The experimental measurements and simulated results of the frequency sweep at a lower level are plotted in Fig. 7(a) and (b), respectively, including the tip displacements, velocities, and voltages across an external resistive load of  $R = 180 \text{ k}\Omega$ . The left column of Fig. 7 plots the upward frequency sweep results, while the right column shows the downward frequency sweep results. The displacement responses in Fig. 7 clearly show that the system only oscillates around the first stable state for both the upward and downward frequency sweep, and the voltage responses are small, in particular for the case of the upward frequency sweep. The numerical integration results in Fig. 7(b) agree well with the measurements for the small-amplitude intra-well oscillations in Fig. 7(a). Fig. 8(a) and (b) plot the experimentally measured and numerically simulated frequency sweep results at a higher excitation level. The snap-through vibrations could be observed from the displacement responses in Fig. 8(a) and (b) for both the upward and downward frequency sweep. Relatively large voltage levels are harvested over the frequency interval of [10.6, 12.3] Hz from the vibrations associated with snap-through responses. However, discrepancies are observed for the global vibrations from Fig. 8(a) and (b). Specifically, the integration results of the downward frequency sweep show a slightly wider frequency bandwidth (10.8-11.8 Hz) of the inter-well vibrations than the

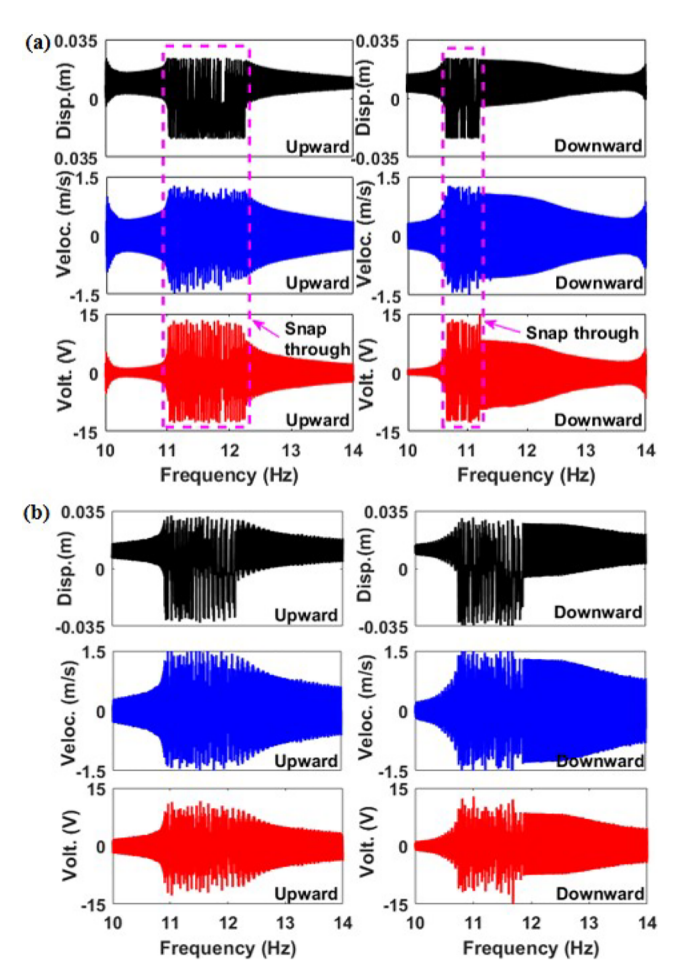


Fig. 8. Frequency sweep experiment results of inter-well vibrations: (a) experiment, (b) simulation.

experimental results (10.6–11.2 Hz). These discrepancies are attributed to the model errors, noise in the measured acceleration excitation, and multiple solutions, especially the error in the measured and fitted force–displacement relation. For instance, the model does not consider the twisting motion of the two sub-beams, which could result in evident errors at higher excitation accelerations.

The pre-displacement  $\Delta$  plays a key role in the bi-stable dynamics of the harvester as qualitatively discussed in the Subsection 3.2. To verify the analysis, frequency sweep experiments were conducted to the prototype with two different pre-displacements, specifically,  $\Delta=2.0$  mm and 2.5 mm. Both the tip velocity and voltage responses of the upward frequency sweep experiments are presented in Fig. 9 for the two pre-displacements. The results show that the frequency range of the large-amplitude snap-through vibration concomitant with higher voltage output is extended from [10.6 12.3] Hz to [10.8 12.9] Hz by the increased pre-displacement constraint. This can be attributed to the deeper potential wells and higher potential energy induced by the larger pre-displacement. In addition, a slight increase in the start frequency of the snap-through motion is also observed from the responses of the harvester with a larger pre-displacement constraint (see Fig. 9).

# 4.2. Harmonic excitations

To investigate the dynamics of the proposed BBPEH, experiments were also carried out under harmonic base acceleration excitations with a frequency of 12 Hz close to the local resonant frequency at different amplitudes. The experiments are firstly performed over varying excitation accelerations at 12 Hz. The peak voltage across a resistor of  $8.2~\mathrm{k}\Omega$  and velocity at each excitation level are collected and plotted in

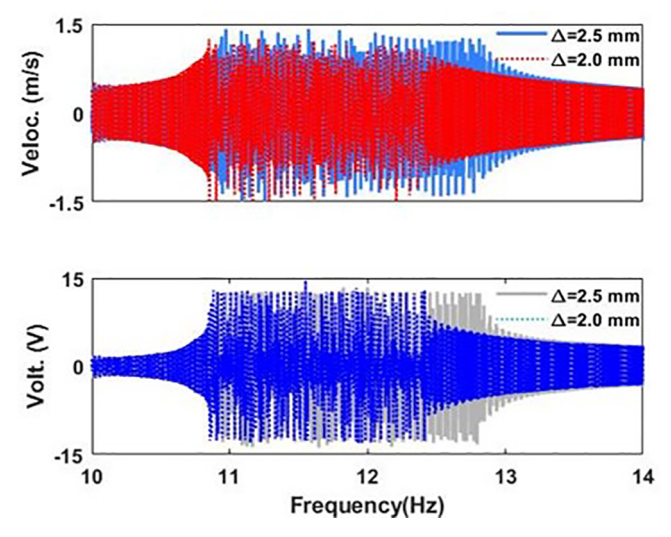


Fig. 9. Influence of the pre-displacement constraint on the dynamics of the system.

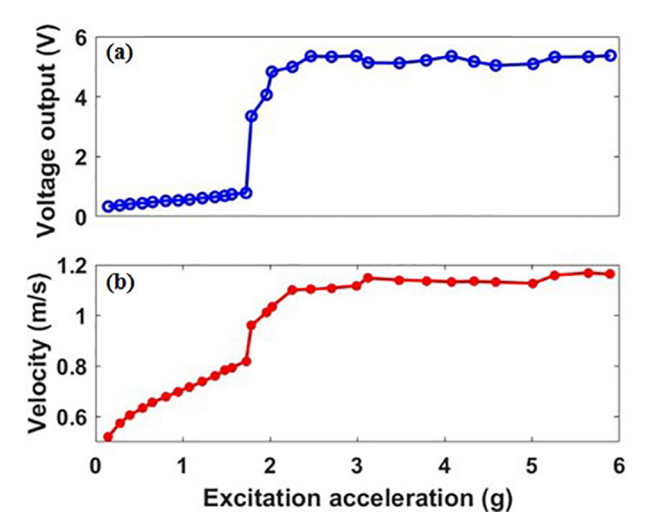


Fig. 10. Bifurgation diagram of (a) the voltage and (b) velocity vs. excitation acceleration.

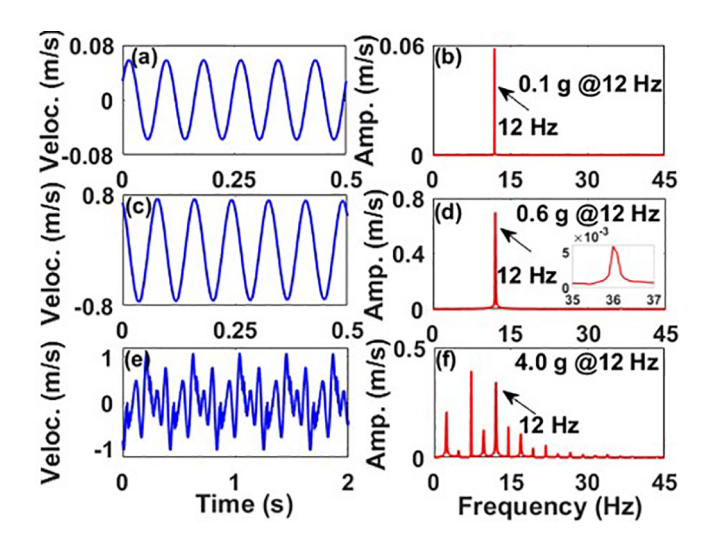
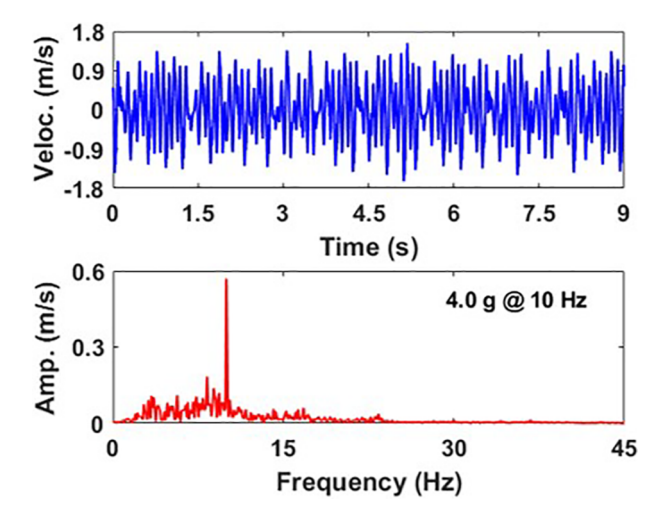


Fig. 11. Time history and FFT of the tip velocity at the excitation frequency of 12 Hz and amplitudes of 0.1 g (a)–(b), 0.6 g (c)–(d), 4.0 g (e)–(f).

the bifurcation diagram in Fig. 10 (a) and (b), respectively, which shows when the excitation acceleration level is greater than 1.8 g the large-amplitude snap through vibrations occur. The plots in Fig. 11(a)–(f) show the time domain velocity responses of the tip mass and the corresponding power spectrum obtained from FFT analysis for the excitation amplitudes of 0.1 g, 0.6 g, and 4.0 g, respectively. Fig. 11(a) and (c) indicate that the tip mass experiences an almost perfect periodic motion at the lower excitation levels of 0.1 g and 0.6 g, and the corresponding power was concentrated at the excitation frequency of 12 Hz, as shown in Fig. 11(b) and (d). The small amplitude superharmonics at 24 Hz and 36 Hz appear due to the nonlinearity at the excitation level of 0.6 g, as shown in the inset in Fig. 11(d). As the excitation amplitude is increased further to 4.0 g, the system experiences the snap-through phenomenon and exhibits very strong nonlinear vibrations, as illustrated in Fig. 11(e), which exhibits relatively large peaks at subharmonics and superharmonics of the excitation frequency. These results also demonstrate that the nonlinear degree of the system increases along with the external excitation level. The power spectrum in Fig. 11(f) shows more peaks over multiple frequencies in addition to the excitation frequency. Syta et al. [20] defined this type of response with clear and distinct peaks in the power spectrum as the multi-frequency regular snap-through response. The snap-through motion of the harvester could become chaotic at different excitation frequencies and levels. As an example, Fig. 12 presents the velocity response and the power spectrum of the harvester under the excitation level of 4.0 g at 10 Hz, where the energy is distributed over a broadband frequency range besides the large amplitude snap-through motion at the excitation frequency. These large-amplitude nonlinear jumps between the two potential wells with continuous spectrum over a wideband frequency range is referred to as the twin-well chaotic snap-through motion [39].

Time-domain voltage responses of the harvester at the excitation frequency of 12 Hz and different excitation levels of 0.1 g, 0.6 g, and 4.0 g are plotted in Fig. 13(a)–(f), along with the power spectrum obtained from FFT analysis. At the lower excitation level of 0.1 g, the time-domain voltage responses and power spectrum presented in Fig. 13(a) and (b) exhibit a periodic motion at a frequency exactly equal to the excitation frequency. Moreover, the system oscillates only in one of the two potential wells under this small excitation level. This vibration is therefore referred to as the single-well period-one motion [39]. As the excitation level is increased to 0.6 g, the time-domain voltage responses in Fig. 13(c) exhibit a period-doubling bifurcation, and two peaks in the power spectrum, at the excitation frequency of 12 Hz and its harmonic at 24 Hz. The second peak at 24 Hz confirms that the quadratic nonlinearity has a significant contribution to the



**Fig. 12.** Time history and FFT of the tip velocity at the excitation frequency of 10 Hz and amplitudes of 4.0 g.

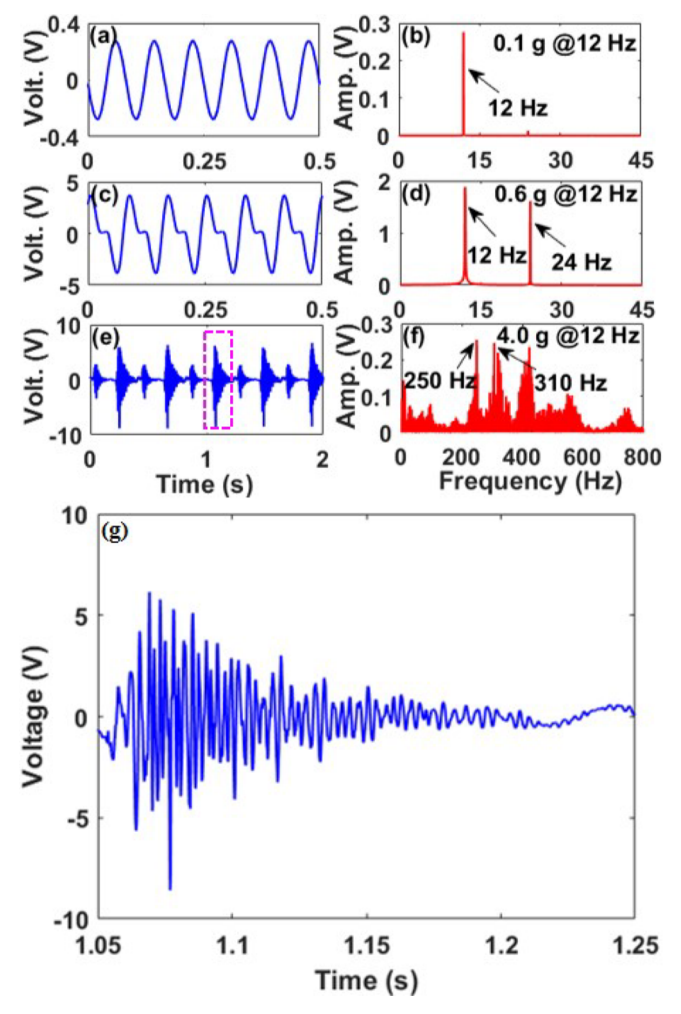
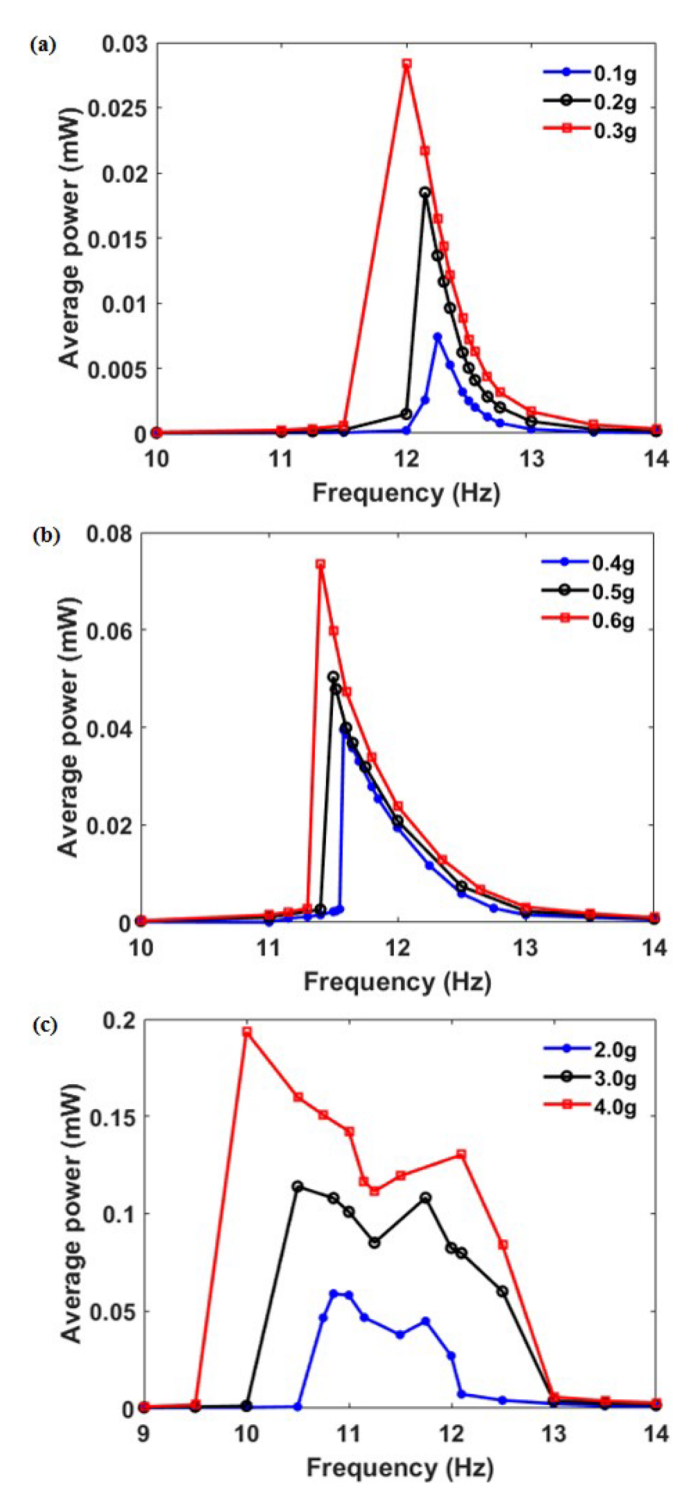


Fig. 13. Time history and FFT of the voltage output at the excitation frequency of 12 Hz and amplitudes of 0.1 g (a)–(b), 0.6 g (c)–(d), 4.0 g (e)–(g).

system dynamics. This conclusion is consistent with the discussion on the experimental results of the force-displacement relationship. It should be noted that this periodic intra-well motion with two dominant frequencies are different from the period-two motion noted by Panyam et al. [39] and Emam et al. [40], where the additional peak of the power spectrum was at the subharmonic of the excitation frequency. The time-domain voltage response in Fig. 13(e) shows the periodic snap-through motion with relatively high frequency vibrations at each snap-through phenomenon, which is not observed from the velocity response of the tip mass in Fig. 11(e). This indicates that the sub-beams of the harvester undergo more complicated local dynamics during the snapping through. This high-frequency response is attributed to the local vibrations of the sub-beam, where the piezoelectric MFC transducer is attached. The high-frequency voltage response during one of the snap-through phenomena, as shown in the dotted box, is expanded in Fig. 13(g). The power spectrum of the voltage response plotted in Fig. 13(f) confirms that the sub-beams experience multiple high-frequency dominated dynamics. The continuously distributed spectrum over the wide frequency range suggests the chaotic motion of the subbeams during the large amplitude inter-well vibrations. This suggests that the proposed BBPEH could extend the effective frequency range over a quite wide bandwidth aside from the single excitation frequency, and therefore generates more power. It should be mentioned that a much lower external resistor of  $8.2\ k\Omega$  was used for the inter-well vibration because of the high-frequency local vibrations during snapping through, instead of the 180  $k\Omega$  used for the case of intra-well vibrations. Nevertheless, the voltage outputs are still much higher than those of the



**Fig. 14.** Average power output of the BBPEH at different excitation levels and frequencies: (a) lower excitation levels, (b) moderate excitation lever, (c) higher excitation levels.

local intra-well vibrations plotted in Fig. 13(a) and (c) even at a much lower resistive load due to the large amplitude inter-well vibrations.

## 4.3. Energy harvesting performance

The energy harvesting performance of the proposed BBPEH is also evaluated in terms of the average power outputs at different excitation levels and frequencies. The average power outputs across the external resistive load of  $R=180~\mathrm{k}\Omega$  at lower excitation levels of 0.1 g, 0.2 g,

and 0.3 g are presented in Fig. 14(a) for different excitation frequencies. It is observed that the power outputs are very small (less than 5  $\mu W$ ) at the excitation frequencies away from the local resonant frequency under the low excitation levels. The power levels increase dramatically as the excitation frequency moves closer to the local resonant frequency. The harvester experienced almost linear local intra-well vibrations at low excitation levels. Fig. 14(b) plots the average power outputs across the same resistor at the moderate excitation levels of 0.4 g, 0.5 g, and 0.6 g. It should be noted that the harvester oscillates around one of the local stable states, and snapp through does not take place under these moderate excitation levels over the frequency ranges of interest. The curves of the average power outputs over different frequencies clearly bend to the left hand, noting the evident soft nonlinearity generally associated with the local vibrations of a bistable system. As the excitation level increases, the frequency bandwidth of the higher power output is also broadened besides the increase in average power output.

At higher excitation levels, the large amplitude inter-well vibrations take place over a certain frequency range, and thus much higher average power could be attained. Since it has been found that the voltage response of the harvester is dominated by the higher frequency components as a result of the snap-through dynamics, the lower load resistance of  $R = 8.2 \text{ k}\Omega$  was used in the experiments. The average power outputs of the harvester at the excitation levels of 2.0 g, 3.0 g, and 4.0 g and frequency varying from 9 Hz to 14 Hz are presented in Fig. 14(c). At the excitation level of 2.0 g, the harvester has a significant large power output over the frequency range of 10.5-12.0 Hz because the large amplitude inter-well vibrations are activated. The harvested power is very small outside of this frequency range due to the small amplitude intra-well dynamics. The frequency bandwidth of the interwell vibration becomes wider as the excitation level increases to 3.0 g and 4.0 g, to respectively cover 10.0-13.0 Hz and 9.5-13.5 Hz. The average power output also evidently increases over these bandwidths. The maximum power output is around 0.193 mW at the excitation of 10 Hz and 4.0 g. This wideband feature of the frequency range in which the harvester could achieve snap-through dynamics accompanied by large power outputs is a key design purpose of nonlinear energy harvesters in practice since ambient environment excitations usually contain frequency components over a wide frequency broadband.

#### 5. Conclusion

Inspired by the rapid shape transition of the Venus flytrap leaves, a novel low-cost, magnet-free, bi-stable piezoelectric energy harvester is designed, prototyped, and tested towards assessing its capability for energy harvesting from broadband vibrations. Different from bi-stable energy harvesters that make use of nonlinear magnetic forces or residual stress in laminate composites, the proposed bio-inspired bi-stable piezoelectric energy harvester (BBPH) takes advantage of the mutual self-constraint at the free ends of two cantilever sub-beams with a predisplacement. This mutual pre-displacement constraint at the free ends curves the two sub-beams in two directions inducing bending and twisting deformations with higher mechanical potential energy in the harvester. The force-displacement curves of the prototype was experimentally measured and numerically fitted by polynomial models. Both frequency sweep and harmonic experiments are conducted on the prototype to study the nonlinear dynamics and to evaluate the energy harvesting performance. The results show that the sub-beams experience much richer local dynamics with multiple high-frequency vibrations compared with the tip mass, even under a single low-frequency harmonic excitation. These local high-frequency vibrations are desirable for a high power output. The average power output of the BBPH shows an increasing trend in both the amplitude and frequency bandwidth as the excitation level increases and is high enough to activate large amplitude inter-well vibrations. Although results were presented for one piezoelectric patch, additional patches that can harvest energy

from other bending and torsion deflections can significantly increase the demonstrated power levels.

#### CRediT authorship contribution statement

Feng Qian: Conceptualization, Methodology, Experiment and simulation, Writing - original draft. Muhammad R. Hajj: Supervision, Writing - review & editing. Lei Zuo: Supervision, Resources, Writing - review & editing.

#### **Declaration of Competing Interest**

The authors declare that they have no known competing financial interests or personal relationships that could have appeared to influence the work reported in this paper.

#### Acknowledgement

The authors gratefully acknowledge the financial support from the National Science Foundation (Award Numbers: 1935951 and 1935954).

#### References

- [1] Zhao LC, Zou HX, Yan G, Liu FR, Tan T, Wei KX, Zhang WM. Magnetic coupling and flextensional amplification mechanisms for high-robustness ambient wind energy harvesting. Energy Convers Manage 2019;201:112166.
- [2] Li Z, Zu J, Yang Z. Introducing hinge mechanisms to one compressive-mode piezoelectric energy harvester. J Renew Sustain Energy 2018;10(3):034704.
- [3] Jiang XY, Zou HX, Zhang WM. Design and analysis of a multi-step piezoelectric energy harvester using buckled beam driven by magnetic excitation. Energy Convers Manage 2017;145:129–37.
- [4] Fan K, Chang J, Chao F, Pedrycz W. Design and development of a multipurpose piezoelectric energy harvester. Energy Convers Manage 2015;96:430–9.
- [5] Wu PH, Chen YJ, Li BY, Shu YC. Wideband energy harvesting based on mixed connection of piezoelectric oscillators. Smart Mater Struct 2017;26(9):094005.
- [6] Daqaq MF, Masana R, Erturk A, Dane Quinn D. On the role of nonlinearities in vibratory energy harvesting: a critical review and discussion. Appl Mech Rev 2014;66(4):040801.
- [7] Harne RL, Wang KW. A review of the recent research on vibration energy harvesting via bistable systems. Smart Mater Struct 2013;22(2):023001.
- [8] Pellegrini SP, Tolou N, Schenk M, Herder JL. Bistable vibration energy harvesters: a review. J Intell Mater Syst Struct 2013;24(11):1303–12.
- [9] Cottone F, Gammaitoni L, Vocca H, Ferrari M, Ferrari V. Piezoelectric buckled beams for random vibration energy harvesting. Smart Mater Struct 2012;21(3):035021.
- [10] And B, Baglio S, Bulsara A, Marletta V. A bistable buckled beam based approach for vibrational energy harvesting. Sens Actuators A 2014;211:153–61.
- [11] Qian F, Zhou S, Zuo L. Approximate solutions and their stability of a broadband piezoelectric energy harvester with a tunable potential function. Commun Nonlinear Sci Numer Simul 2020;80:104984.
- [12] Harne RL, Thota M, Wang KW. Bistable energy harvesting enhancement with an auxiliary linear oscillator. Smart Mater Struct 2013;22(12):125028.
- [13] Ferrari M, Ferrari V, Guizzetti M, And B, Baglio S, Trigona C. Improved energy harvesting from wideband vibrations by nonlinear piezoelectric converters. Sens Actuators A 2010;162(2):425–431. Eurosensors XXIII, 2009.
- [14] Stanton SC, McGehee CC, Mann BP. Nonlinear dynamics for broadband energy harvesting: Investigation of a bistable piezoelectric inertial generator. Physica D 2010;239(10):640–53.
- [15] Zhou S, Cao J, Erturk A, Lin J. Enhanced broadband piezoelectric energy harvesting using rotatable magnets. Appl Phys Lett 2013;102(17):173901.
- [16] Cao J, Zhou S, Inman DJ, Lin J. Nonlinear dynamic characteristics of variable inclination magnetically coupled piezoelectric energy harvesters. J Vib Acoust 2015;137(2):021015.
- [17] Zou HX, ming Zhang W, Li WB, Wei KX, Gao QH, Peng ZK, Meng G. Design and experimental investigation of a magnetically coupled vibration energy harvester using two inverted piezoelectric cantilever beams for rotational motion. Energy Convers Manage 2017;148:1391 – 1398.
- [18] Arrieta AF, Delpero T, Bergamini AE, Ermanni P. Broadband vibration energy harvesting based on cantilevered piezoelectric bi-stable composites. Appl Phys Lett 2013;102(17):173904.
- [19] Li Y, Zhou S, Yang Z, Guo T, Mei X. High-performance low-frequency bistable vibration energy harvesting plate with tip mass blocks. Energy 2019;180:737–50.
- [20] Syta A, Bowen CR, Kim HA, Rysak A, Litak G. Experimental analysis of the dynamical response of energy harvesting devices based on bistable laminated plates. Meccanica 2015;50(8):1961–70.
- [21] Syta A, Bowen CR, Kim HA, Rysak A, Litak G. Responses of bistable piezoelectriccomposite energy harvester by means of recurrences. Mech Syst Sig Process

- 2016:76-77:823-32.
- [22] Firouzian-Nejad A, Bowen C, Mustapha S, Ghayour M, Ziaei-Rad S. Bi-stable hybrid composite laminates containing metallic strips: an experimental and numerical investigation. Smart Mater Struct 2019;28(5):055030.
- [23] Firouzian-Nejad A, Mustapha S, Ziaei-Rad S, Ghayour M. Characterization of bistable pure and hybrid composite laminates—an experimental investigation of the static and dynamic responses. J Compos Mater 2019;53(5):653–67.
- [24] Pan D, Li Y, Dai F. The influence of lay-up design on the performance of bi-stable piezoelectric energy harvester. Compos Struct 2017;161:227–36.
- [25] Pan D, Jiang W, Dai F. Dynamic analysis of bi-stable hybrid symmetric laminate. Compos Struct 2019;225:111158.
- [26] Kim GW, Kim J. Compliant bistable mechanism for low frequency vibration energy harvester inspired by auditory hair bundle structures. Smart Mater Struct 2012;22(1):014005.
- [27] Wang W, He X, Wang X, Wang M, Xue K. A bioinspired structure modification of piezoelectric wind energy harvester based on the prototype of leaf veins. Sens Actuators A 2018;279:467–73.
- [28] Wang W, Wang X, He X, Wang M, Shu H, Xue K. Comparisons of bioinspired piezoelectric wind energy harvesters with different layout of stiffeners based on leaf venation prototypes. Sens Actuators A 2019;298:111570.
- [29] Fu H, Sharif-Khodaei Z, Aliabadi F. A bio-inspired host-parasite structure for broadband vibration energy harvesting from low-frequency random sources. Appl Phys Lett 2019;114(14):143901.
- [30] Zhang Y, Jeong CK, Yang T, Sun H, Chen LQ, Zhang S, Chen W, Wang Q. Bioinspired elastic piezoelectric composites for high-performance mechanical energy harvesting. J Mater Chem A 2018;6(30):14546–52.
- [31] Kim SW, Koh JS, Lee JG, Ryu J, Cho M, Cho KJ. Flytrap-inspired robot using

- structurally integrated actuation based on bistability and a developable surface. Bioinspir Biomimet 2014;9(3):036004.
- [32] Zhang Z, Chen D, Wu H, Bao Y, Chai G. Non-contact magnetic driving bioinspired venus flytrap robot based on bistable anti-symmetric cfrp structure. Compos Struct 2016;135:17–22.
- [33] Kim P, Son D, Seok J. Triple-well potential with a uniform depth: advantageous aspects in designing a multi-stable energy harvester. Appl Phys Lett 2016;108(24):243902.
- [34] Zhou S, Cao J, Inman DJ, Liu S, Wang Z. Broadband tristable energy harvester: modeling and experiment verification. Appl Energy 2014;133:33–9.
- [35] Pan D, Dai F. Design and analysis of a broadband vibratory energy harvester using bi-stable piezoelectric composite laminate. Energy Convers Manage 2018;169:149–60.
- [36] Neville RM, Groh RMJ, Pirrera A, Schenk M. Shape control for experimental continuation. Phys Rev Lett 2018;120:254101.
- [37] Wang W, Cao J, Bowen CR, Inman DJ, Lin J. Performance enhancement of non-linear asymmetric bistable energy harvesting from harmonic, random and human motion excitations. Appl Phys Lett 2018;112(21):213903.
- [38] He Q, Daqaq MF. Influence of potential function asymmetries on the performance of nonlinear energy harvesters under white noise. J Sound Vib 2014;333(15):3479–89.
- [39] Panyam M, Daqaq MF, Emam SA. Exploiting the subharmonic parametric resonances of a buckled beam for vibratory energy harvesting. Meccanica 2018;53(14):3545–64.
- [40] Emam SA, Hobeck J, Inman DJ. Experimental investigation into the nonlinear dynamics of a bistable laminate. Nonlinear Dyn 2019;95(4):3019–39.